ACES Asian Chemical Editorial Society

DOI: 10.1002/asia.202000635

CHEMISTRY AN ASIAN JOURNAL Full Paper

Special Collection

New D-A-A′-Configured Small Molecule Donors Employing Conjugation to Red-shift the Absorption for Photovoltaics

Chun-Kai Wang,[a] Xiaozhou Che,[b] Yuan-Chih Lo,[a] Ya-Ze Li,[c] Yung-Hao Wang,[c] Stephen R. Forrest,*[b] Shun-Wei Liu,*[c, d] and Ken-Tsung Wong*[a, e]

Abstract: Four new donor-acceptor-acceptor′ (D-A-A′)-configured donors, **CPNT**, **DCPNT**, **CPNBT**, and **DCPNBT** equipped with naphtho[1,2-*c*:5,6-*c*′]bis([1,2,5]-thiadiazole) (NT) or naphtho[2,3-*c*][1,2,5]thiadiazole (NBT) as the central acceptor (A) unit bridging triarylamine donor (D) and cyano or dicyanovinylene acceptor (A′), were synthesized and characterized. All molecules exhibit bathochromic absorption shifts as compared to those of the benzothiadiazole (BT)-based analogues owing to improved electron-withdrawing and quinoidal character of NT and NBT cores that lead to stronger intramolecular charge transfer. Favorable energy level alignments with C_{70}, together with the good thermal stability and the antiparallel dimeric packing render **CPNT** and **DCPNT** suitable donors for vacuum-processed organic photovoltaics (OPV)s. OPVs based on **DCPNT**:C_{70} active layers displayed the best power conversion efficiency (PCE) = 8.3%, along with an open circuit voltage of 0.92 V, a short circuit current of 14.5 mA cm^{-2} and a fill factor of 62% under 1 sun intensity, simulated AM1.5G illumination. Importantly, continuous light-soaking with AM 1.5G illumination has verified the durability of the devices based on **CPNT**:C_{70} and **DCPNT**:C_{70} as the active blends. The devices were examined for their feasibility of indoor light harvesting under 500 lux illumination by a TLD-840 fluorescent lamp, giving *PCE* = 12.8% and 12.6%, respectively. These results indicate that the NT-based D-A-A′-type donors **CPNT** and **DCPNT** are potential candidates for high-stability vacuum-processed OPVs suitable for indoor energy harvesting.

Introduction

Organic photovoltaics (OPVs) that possess mechanical flexibility, lightweight and high efficiency are emerging as promising means for renewables.[1–5] Over the past two decades, studies have concentrated on the development of active materials as well as device engineering for boosting the power conversion efficiency (*PCE*). Typically, the active layer of an efficient OPV is composed of a p-type donor and an n-type acceptor for creating a bulk heterojunction (BHJ) that can maximize the conversion of absorbed photons into electric current. A significantly wide range of organic materials including oligomers and polymers have been tailor-made as donors to work with fullerene-based acceptors. For example, Chen and coworkers reported *PCE* = 10.08% with the BHJ composed of a functional oligothiophene **DRCN5T** (Figure 1) as donor and $PC_{71}BM$ as acceptor.[6] In addition, Wei and coworkers reported a benzo[1,2-*b*:4,5-*b*′]dithiophene (BDT)-based donor **BTID-2F** (Figure 1) that blended with $PC_{71}BM$ to serve as a BHJ for OPVs with an average *PCE* = 11.08%.[7] These representative small-molecule donors possess advantages such as high batch-to-batch reproducibility and feasible purification owing to the well-defined molecular structures. However, the structural skeletons limit the space for the sophisticated tuning of physical characteristics, particularly the morphological ordering of the active layer. On the other hand, polymer donors made of suitable monomers represent examples as donors mainly due to the morphological features that lead to improved carrier separation and transport, leading to higher short-circuit current densities (J_{sc}) and fill factors (*FF*s) as compared to those of small-molecule donors. For example, Yan and coworkers developed quaterthiophene-based polymer donors to blend with fullerene derivatives for OPVs with *PCE*s > 10%.[8] By tuning the side chain structures, the donor **PffBT4T–C_9C_{13}** (Figure 1) blended with $PC_{71}BM$ allows *PCE* = 11.7%[9]. However, fullerene derivatives exhibit low absorbance in the visible region, limiting the light-harvesting window. In addition, the lowest unoccupied molecular orbitals (LUMOs) of fullerenes are relatively inert

[a] Dr. C.-K. Wang, Y.-C. Lo, Prof. Dr. K.-T. Wong
Department of Chemistry
National Taiwan University
Taipei 10617 (Taiwan)
E-mail: kenwong@ntu.edu.tw

[b] Dr. X. Che, Prof. Dr. S. R. Forrest
Departments of Electrical Engineering
Material Science and Engineering and Physics
University of Michigan
Ann Arbor, Michigan 48109 (USA)
E-mail: stevefor@umich.edu

[c] Y.-Z. Li, Y.-H. Wang, Prof. Dr. S.-W. Liu
Organic Electronics Research Center
Ming Chi University of Technology
New Taipei City 24301 (Taiwan)
E-mail: swliu@mail.mcut.edu.tw

[d] Prof. Dr. S.-W. Liu
Department of Electronic Engineering
Ming Chi University of Technology
New Taipei City 24301 (Taiwan)

[e] Prof. Dr. K.-T. Wong
Institute of Atomic and Molecular Science
Academia Sinica
Taipei 10617 (Taiwan)

Supporting information for this article is available on the WWW under https://doi.org/10.1002/asia.202000635

This manuscript is part of a special collection for the 20th Anniversary of the Tateshina Conference.

against the structural functionalization, restricting the selection of polymer donors and thus limiting progress. Thanks to the development of non-fullerene acceptors (NFAs), OPV efficiencies have made dramatic improvements. NFAs with tunable energy levels lead to absorption spanning from the visible to near infrared (NIR) region. An NFA mixed with a judiciously selected polymeric donor gives the device control of the BHJ morphology and thus higher J_{sc} as well as open circuit voltage (V_{oc}).[10–14] Among many types of NFAs, small molecules with acceptor-donor-acceptor (A-D-A)-configuration are the most successful at achieving high efficiency. For example, Zhan and coworkers first reported an A-D-A-configured NFA **IEIC** (Figure 1) with indacenodithiophene (IDT) as the central electron-donating core end-capped with electron-accepting (3-oxo-2,3-dihydro-1*H*-inden-1-ylidene)malononitrile (ID). The device based on a BHJ blend comprising a low bandgap polymer donor **PTB7−Th** (Figure 1) and **IEIC** exhibited *PCE* = 6.31%.[15] This triggered rapid advances of NFAs for binary OPVs to deliver *PCE*s > 16%.[16–21] Strikingly, an OPV device with a *PCE* up to 18% was achieved by a blend comprising dithieno[3′,2′:3,4;2″,3″:5,6]benzo[1,2-*c*][1,2,5] thiadiazole (DTBT)-based polymer donor **D18** (Figure 1) and an NFA **Y6** (Figure 1) with fused thienothienopyrrolo-thienothienoindole (TTP-TTI) core.[22] The success of introducing NFAs as the essential component in the active layer paves the way toward practical applications of OPVs. These examples are fabricated with solution-processed techniques, leaving prominent issues such as the morphological stability of the BHJ blend as well as the durability of large area modules as the main challenges remaining to be conquered.[23]

Compared to the solvent-based fabrication, the vacuum-deposition technique for optoelectronics provides highly accurate and controllable layer thickness, simplified processing of multilayer devices, and homogeneous films demonstrated by the successful commercialization of organic light-emitting diodes (OLEDs).[24] More importantly, an extremely stable vacuum-deposited OPV device employing a small molecule donor 5,10,15,20-Tetraphenylbisbenz[5,6]indeno[1,2,3-*cd*:1′,2′,3′-*lm*]perylene (DBP) and acceptor C_{70} showed an extrapolated intrinsic lifetime more than 4.9×10^7 h determined by a 20% reduction of its initial *PCE* under high-intensity illumination was recently reported by Forrest *et al.*[25] The favorable features of vacuum-deposited OPVs are continuing to attract attention on developing novel materials for improving the *PCE* without sacrificing device stability. Small molecules with limited π-conjugated backbones with small lateral groups ensuring sufficient solubility for purification as well as the thermal stability are designed to limit the molecular weight such that they are suitable for vacuum-deposition. As a result, more sophisticated molecular designs are necessary to furnish light-harvesting capability in the visible or even the NIR region.

Previously, we reported a D-A-A′-configured donor molecule, **DTCPB**, in which the electron-deficient core benzo[*c*][1,2,5]-thiadiazole (BT) bridging the electron-donating triarylamine and the electron-withdrawing cyano group.[26] The high quinoidal character of BT together with the strong D and A combination induce efficient intramolecular charge transfer (ICT) absorption in the visible wavelength. In addition, the suitable energy level alignment with respect to fullerenes, and the antiparallel dimeric packing for reducing the bulk dipole render **DTCPB** a good candidate donor for an OPV device achieving a *PCE* = 7.0% under 1 sun illumination with high stability, and *PCE* = 13–16% under 200 to 1200 lux illumination of a TLD-840 fluorescent lamp. The absorption of **DTCPB** can be bathochromically shifted by replacing the end-capping CN group with a dicyanovinylene (DCV) group. Indeed, the DCV-end capped counterpart **DTDCPB** exhibits red-shifted absorption owing to enhanced ICT as compared to that of **DTCPB**.[27] As a result, the **DTDCPB**-based OPV device exhibited a higher J_{sc} value and *PCE* = 9.8%, representing the best single junction OPV device reported by vacuum-process.[28] These results highlight the importance of developing D-A-A′-configured molecules with the spectral coverage extended to longer wavelengths for improved light harvesting efficiency. This motivates us to implement the *conjugation effect* on the molecular skeleton as the main approach for shifting the absorption spectrum. As compared to the BT unit, naphtho[1,2-*c*:5,6-*c*′]bis([1,2,5]-thiadiazole) (NT) and naphtho[2,3-*c*][1,2,5]thiadiazole (NBT) (Scheme 1) present elongated π-conjugation in parallel and orthogonal directions along the molecular conjugated backbone, respectively. Takimiya and coworkers reported a D-A-type copolymer, **PNTz4T** (Figure 1), comprising quaterthiophene as electron-rich moiety and NT as electron-deficient moiety,[29] exhibited red-shifted absorption and improved intermolecular interactions compared to those of the BT-based analogue **PBTz4T**. Thus, the **PNTz4T**-based device displayed a higher *PCE* = 6.3% as compared to that of **PBTz4T** (2.6%). Furthermore, a series of devices based on NT-based polymeric donors exhibited *PCE* > 8% through electron-rich moiety and alkyl chain modification were reported,[30–32] indicating the superiority of NT as electron-deficient moiety in D-A-type conjugated systems. On the other hand, NBT-based molecules were incorporated as red-to-NIR emitters in OLEDs.[33–34] There are rather limited examples of NBT-based polymers or small molecules for OPVs.[35–36] In this work, a new synthetic pathway was devised for incorporating NT and NBT as the central A units of D-A-A′-configured small molecule donors **CPNT**, **CPNBT**, **DCPNT** and **DCPNBT** (Scheme 1). These D-A-A′-type molecules were characterized and compared to those of BT-based counterparts **DTCPB** and **DTDCPB**, establishing a clear structure-property relationship. The stronger electron-deficiency of NT and NBT together with the conjugation effect introduced on the molecular skeletons leads to red-shifted absorption compared to the BT-based parent molecules. The reduced optical energy gaps are ascribed to the lower LUMO energy levels and stronger ICT characters of these new D-A-A′-type molecules. Among them, **DCPNBT** exhibits the most red-shifted absorption (λ_{onset} = 722 nm) approaching to the NIR region. The photovoltaic characteristics of vacuum-deposited OPVs with the active blends comprising these donors and C_{70} were explored. The devices employed NT-based D-A-A′-type donors outperform the ones based on NBT as the A units. Among these blends, the device based on **DCPNBT** gives inferior performance, which can be ascribed to the twisted conformations observed by X-ray crystallography analysis that impede inter-

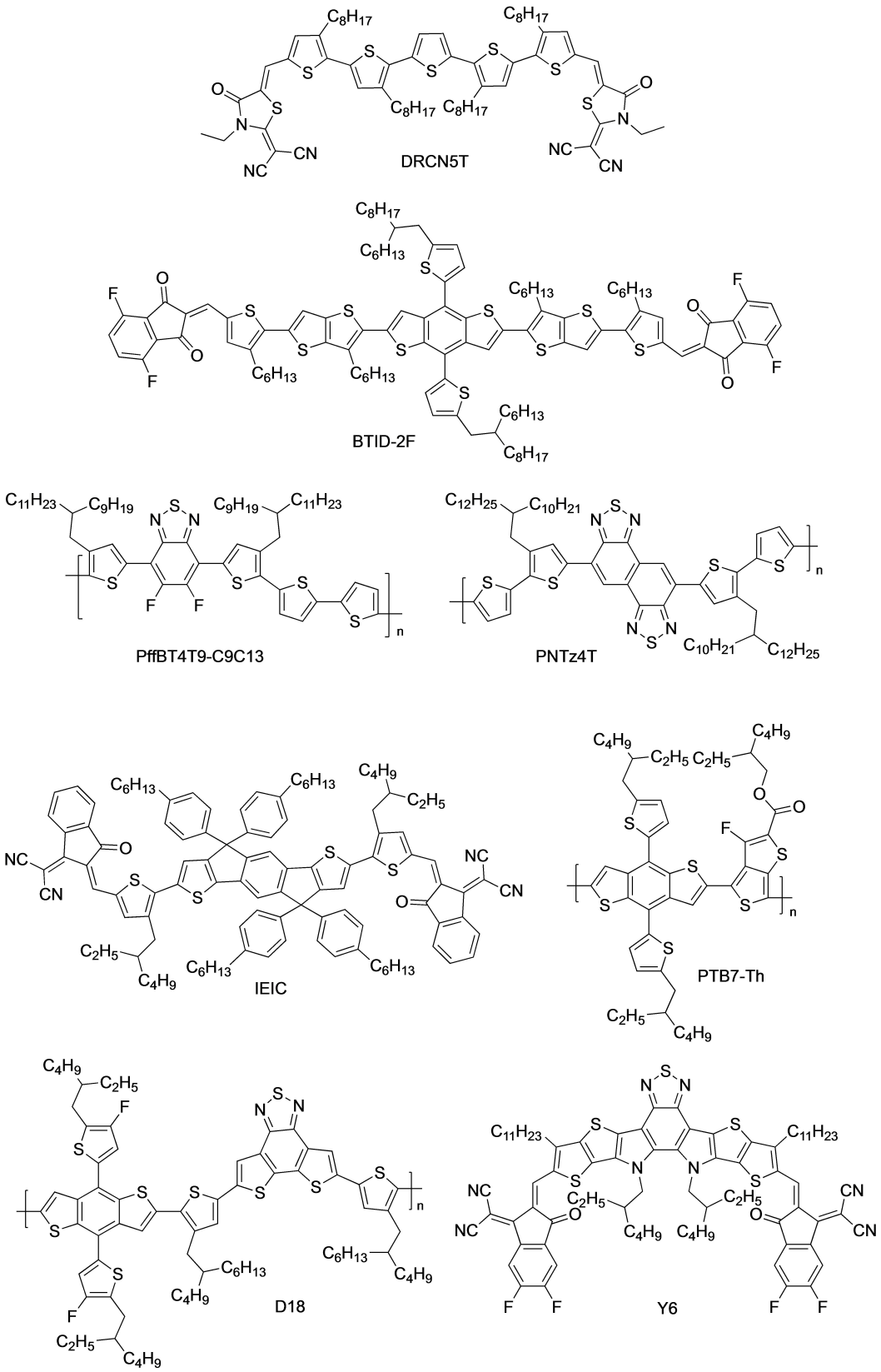

Figure 1. The chemical structures of the discussed donors and non-fullerene acceptors.

molecular interactions. After optimization, the device with **DCPNT**:C_{70} as the active layer displayed the best *PCE* = 8.30%, along with a V_{oc} = 0.92 V, a J_{sc} = 14.5 mA cm^{-2} and a *FF* = 62%. Furthermore, the stabilities of the devices based on **CPNT**:C_{70}

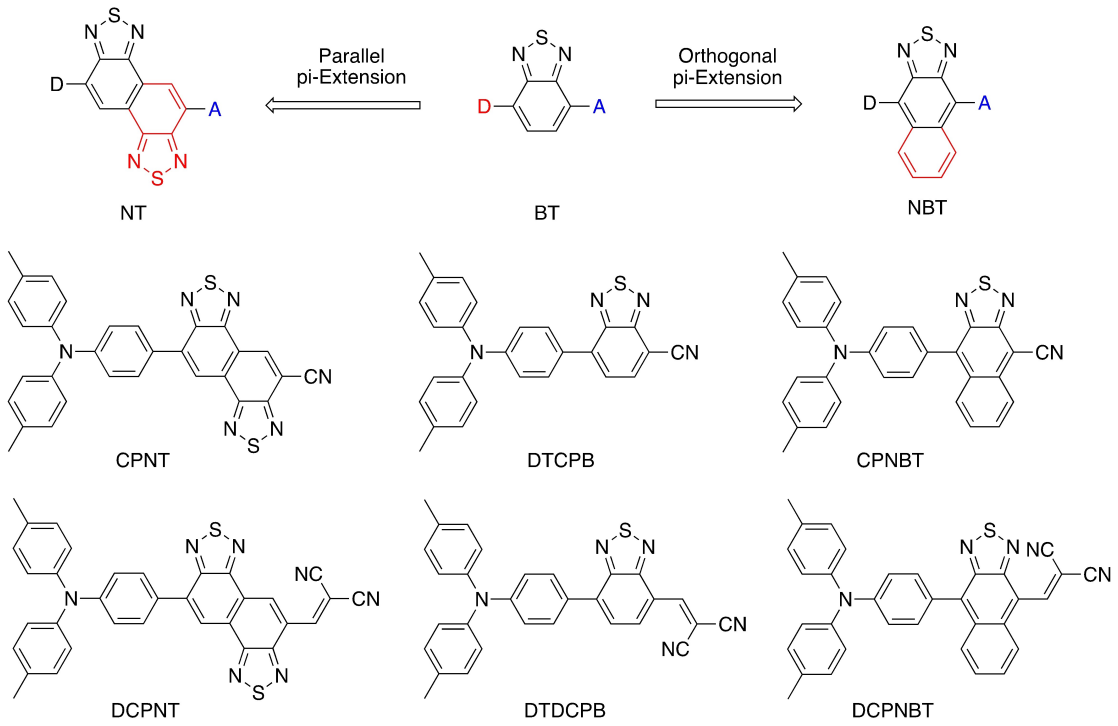

Scheme 1. Molecular design strategy of replacing electron-deficient moiety BT to NT/NBT, and molecular structures of **DTCPB**, **CPNT**, **CPNBT**, **DTDCPB**, **DCPNT** and **DCPNBT**.

and **DCPNT**:C_{70} as the active blends were examined with continuous light-soaking under AM 1.5G illumination. The **CPNT**- and **DCPNT**-based devices were further explored for their use in indoor light harvesting under 500 lux illumination of a TLD-840 fluorescent lamp, giving *PCE* = 12.64% and 12.50%, respectively. These results indicate that the new NT-based D-A-A′-type donors **CPNT** and **DCPNT** are potential candidates for high-stability vacuum-processed OPVs that are suitable for indoor light energy scavenging.

Results and Discussions

The synthetic routes for D-A-A′-configured molecules **CPNT**, **CPNBT**, **DCPNT** and **DCPNBT** are shown in Scheme 2. Starting from 5,10-dibromonaphtho[1,2-*c*:5,6-*c*′]bis([1,2,5]thiadiazole) (**1**)[37] and 4,9-dibromonaphtho[2,3-*c*][1,2,5]thiadiazole (**2**)[36], the Pd(0)-catalyzed Suzuki-Miyaura reaction with alkene boronic ester (**3**) freshly prepared by the hydroboration of 1-hexyne with catecholborane afforded the mono alkenyl substituted intermediates **4** and **5**, respectively. The ozonolysis of **4** and **5** at −78 °C followed by the treatment of dimethyl sulfide gave the crucial bromo-aldehyde intermediates **6** and **7**, respectively. Subsequently, Pd(II)-catalyzed Stille cross coupling of intermediates **6** and **7** with freshly prepared 4-methyl-*N*-(*p*-tolyl)-*N*-(4-(trimethylstannyl)phenyl)aniline gave the aldehydes **8** and **9** with 75% and 78% of isolated yield, respectively. The DCV group was introduced by Knoevenagel condensation of **8** and **9** with malononitrile in the presence of triethylamine gave the final targets **DCPNT** and **DCPNBT**. For the CN-substituted targets **CPNT** and **CPNBT**, the dibromo starting substrates **1** and **2** underwent Pd(II)-catalyzed Stille cross-coupling with 1 equivalent of freshly prepared 4-methyl-*N*-(*p*-tolyl)-*N*-(4-(trimethylstannyl)phenyl)aniline to afford intermediates **10** and **11**, respectively. The final targets **CPNT** and **CPNBT** were achieved by microwave-assisted cyanation of intermediate **10** and **11** with copper cyanide. All new molecules were characterized with NMR and HRMS with satisfactory data. The thermal stability was analyzed by thermogravimetric analysis (TGA) (Figure S1a), the data are summarized in Table 1. Except for **DCPNBT**, the decomposition temperature, $T_{d,}$ (corresponding to 5% weight loss) under N_2 of **CPNNT**, **CPNBT** and **DCPNT** is higher compared to that of BT-based counterparts. The relative low T_d found for **DCPNBT** implies the potential risk for decomposition during the vacuum-evaporation. In addition, the morphological property was examined with the differential scanning calorimetry (DSC) analysis (Figure S1b). However, no glass transition and crystallization signals can be detected for **DCPNT** and **DCPNBT**. On the other hand, during the heating process, a crystallization temperature (T_c) and melting temperature (T_m) for **CPNBT** was detected at 170 °C and 234 °C, respectively. For **CPNT**, a T_m at 278 °C during the heating process, and a T_c at 239 °C during the cooling process was detected.

Figure 2a depicts the electronic absorption spectra of new D-A-A′-type molecules **CPNT**, **CPNBT**, **DCPNT** and **DCPNBT** in CH_2Cl_2 solution (10^{-5} ~ 10^{-7} M). The corresponding data are summarized in Table 1. The broad and structureless absorption peaks in the long-wavelength regions are attributed to the ICT transition, whereas the absorption peaks in the region of 250–

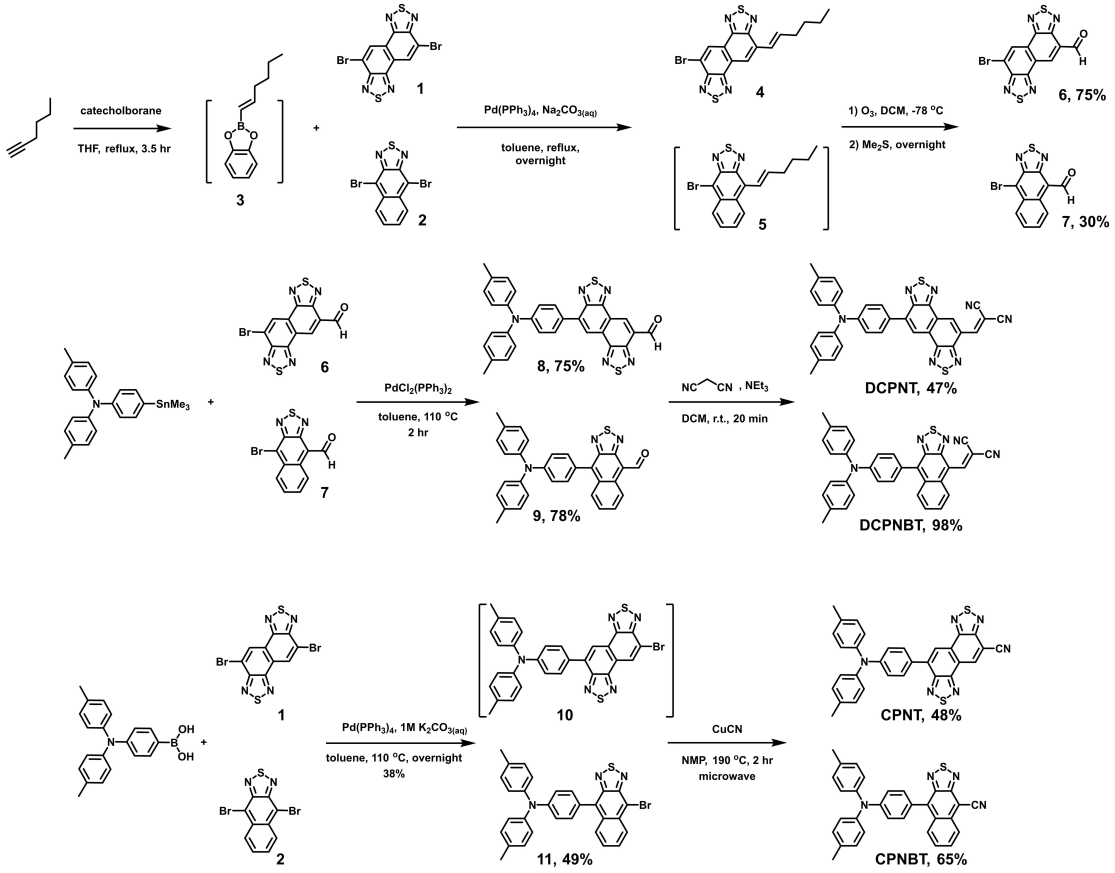

Scheme 2. Synthetic routes of new D-A-A′-type donors **CPNT**, **CPNBT**, **DCPNT** and **DCPNBT**.

Table 1. Photophysical, electrochemical and thermal properties of **DTCPB**[26], **CPNT**, **CPNBT**, **DTDCPB**[27], **DCPNT** and **DCPNBT**.

Molecule	λ_{ICT} [nm][a]	λ_{onset} [nm][b]	ε [$M^{-1}cm^{-1}$][a]	HOMO [eV][c]	LUMO [eV][c]	T_d [°C]
DTCPB	491	573	18200	−5.26	−3.22	287
CPNT	534	622	17000	−5.24	−3.44	353
CPNBT	570	672	11200	−5.26	−3.54	307
DTDCPB	570	669	27400	−5.27	−3.62	308
DCPNT	589	704	25000	−5.25	−3.74	339
DCPNBT	599	722	12500	−5.25	−3.72	278

[a] In dichloromethane solution. [b] Calculated from the onset of absorption spectra in dichloromethane solution. [c] HOMO = $-e(E_{oxi}^{1/2}-E_{Fc}^{1/2}+4.8\ V)$; LUMO = $-e(E_{red}^{1/2}-E_{Fc}^{1/2}+4.8\ V)$.

450 nm are assigned to π-π* transition. The replacement of the central BT core in D-A-A′ skeleton with more electron-deficient NT moiety enhances the ICT character, leading to a red-shifted ICT transition absorption peak (λ_{ICT}) for **CPNT** (534 nm, extinction coefficient (ε) = 17000 $M^{-1}cm^{-1}$) and **DCPNT** (589 nm, ε = 25000 $M^{-1}cm^{-1}$) as compared to those of parent compounds **DTCPB** (491 nm, ε = 18200 $M^{-1}cm^{-1}$) and **DTDCPB** (570 nm, ε = 27400 $M^{-1}cm^{-1}$). In addition, the NBT-based molecules **CPNBT** and **DCPNBT** show the most red-shifted λ_{ICT} of 570 and 599 nm but with obviously low extinction coefficient of 11200 and 12500 $M^{-1}cm^{-1}$, respectively. The electrochemical characteristics of NT- and BT-based D-A-A′ molecules were studied by cyclic voltammetry. Figure 2b depicts the cyclic voltammograms of **CPNT**, **CPNBT**, **DCPNT** and **DCPNBT** and the data are summarized in Table 1. One reversible oxidation potential was found for each molecule: **CPNT** (0.44 V), **CPNBT** (0.46 V), **DCPNT** (0.45 V), and **DCPNBT** (0.45 V), which is assigned to the oxidation of the triarylamine moiety. On the other hand, the first reversible reduction potential of **CPNT** (−1.36 V) and **CPNBT** (−1.26 V) is assigned to the reduction of electron-deficient NT and NBT moieties coupled to the end-capped CN group. The coupling of a stronger electron-deficient group DCV to NT and NBT units leads **DCPNT** and **DCPNBT** to have lower reduction potential observed at −1.06 V and −1.08 V, respectively, as compared to those of **CPNT** and **CPNBT**. Apparently, the reduction propensity of NBT-based molecules **CPNBT** and **DCPNBT** is higher than those of NT-based ones **CPNT** and **DCPNT**, indicating the more electron-deficient character of the NBT moiety. Refer to the

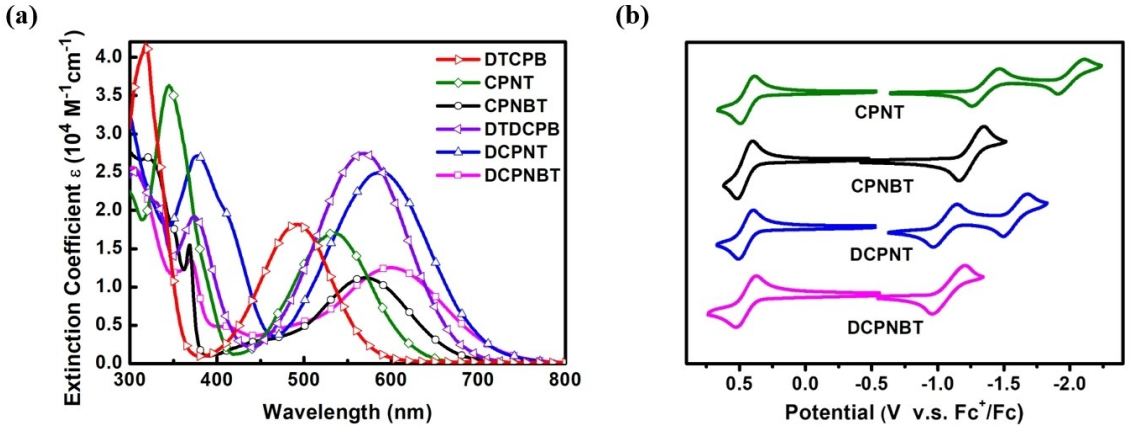

Figure 2. (a) UV-vis spectra of **DTCPB**, **CPNT**, **CPNBT**, **DTDCPB**, **DCPNT** and **DCPNBT** in CH_2Cl_2. (b) Cyclic voltammograms of **CPNT**, **CPNBT**, **DCPNT** and **DCPNBT** in CH_2Cl_2 (oxidation) and THF (reduction).

ferrocene (Fc)/ferrocenium (Fc^+) redox couple, the energy levels of the highest occupied molecular orbitals (HOMOs) and LUMOs were calculated from the oxidation and reduction potentials, respectively. The HOMO/LUMO energy levels of **CPNT**, **CPNBT**, **DCPNT** and **DCPNBT** are −5.24 eV/−3.44 eV, −5.26 eV/−3.55 eV, −5.25 eV/−3.74 eV and −5.25 eV/−3.72 eV, respectively. The HOMO energy levels are relatively insensitive to the electronic features of the central BT, NT, and NBT units. However, the LUMO levels of **CPNT** and **CPNBT** are obviously lower than that of **DTCPB** (−3.22 eV) while the LUMO levels of **DCPNT** and **DCPNBT** are lower than that of **DTDCPB** (−3.62 V). These results indicate that the optical energy gaps of these new D-A-A′ molecules as compared to those of BT-based parent molecules are governed by the NT and NBT cores incorporated into the D-A-A′ configuration. The results reveal that the effect of introducing NBT onto the D-A-A′ architecture for an orthogonal extension of π-conjugation is more pronounced as compared to that of NT unit with the parallel π-extension of the D-A-A′ skeleton.

Crystals of new D-A-A′-type molecules **CPNT**, **DCPNT**, **CPNBT** and **DCPNBT** suitable for single X-ray diffraction analyses were obtained from the bilayer (CH_2Cl_2 or $CHCl_3$ as dissolving solvent and hexane or methanol as orthogonal solvent) diffusion method. The crystals data are summarized in Table S1 and S2 (Supporting Information, SI). As shown in Figure 3, the CN-capped molecules **CPNT** and **CPNBT** show similar dihedral angles of 40.37° and 40.43°, between the phenylene (Ph) ring and the central electron deficient core NT ring and NBT ring, respectively. It is interesting to see that dicyanovinylene (DCV)-substituted **DCPNT** exhibits the dihedral angle of 15.49° respect to the Ph/NT and 1.77° between the NT ring and the DCV moiety. **DCPNT** shows smaller dihedral angles for the inter-planes of Ph ring/NT ring and NT ring/DCV moiety, being comparable to the corresponding dihedral angles of **DTDCPB** reported by Chen *et. al.*[27] and Ting *et. al.*,[26] indicating the more planar molecular conformation induced by the NT unit. The elongated π-conjugation together with the stronger ICT induced by the coplanar conformation lead **CPNT** and **DCPNT** to have red-shifted absorption and an increased ε. In contrast, the corresponding dihedral angles of **DCPNBT** are significantly larger, for example, 45.63° between the Ph ring and the NBT ring and 46.67° between the NBT ring and the DCV moiety. Apparently, **CPNBT** and **DCPNBT** exhibit more twisted conformations due to steric interactions between the Ph ring and the Ph ring orthogonally fused to the BT core. The highly twisted conformations of NBT-based molecules decrease the HOMO and LUMO overlaps, which lead to the smaller extinction coefficients of the ICT absorptions observed for **CPNBT** and **DCPNBT**.

The bond length between the phenylene ring and NT ring (C2-C3) is 1.462 Å for **CPNT**, and 1.460 Å for **DCPNT**, and 1.479 Å for **CPNBT** and 1.477 Å for **DCPNBT**. The bond length alternation (BLA) of the C2-C3 bonds were calculated according to the literature[38] is 0.070 Å, 0.061 Å, 0.072 Å and 0.070 Å for **CPNT**, **DCPNT**, **CPNBT** and **DCPNBT**, respectively, which are smaller than the BLA of **DTCPB** (0.081 Å) and **DTDCPB** (0.083 Å). The smaller BLA of NT- and NBT-based derivatives as compared to those of parent BT-based **DTCPB** and **DTDCPB** implies that the phenylene ring exhibits improved π conjugation with NT and NBT rings than with BT ring, which is beneficial for inducing larger ICT. However, the bond length (1.435 Å) between the NT ring and dicyanovinylene group of **DCPNT** is shorter than that (1.455 Å) of **DCPNBT**. The longer bond length implies weaker bond strength between the NBT and the DCV moiety of **DCPNBT**, which is plausibly responsible for the poorer thermal stability. It is generally accepted that materials with close, ordered intermolecular packing are advantageous for charge carrier transport. Owing to the highly polar nature induced by the D-A-A′ configuration, all these molecules showed antiparallel dimeric packing with the inter-plane π–π distance between 3.3 Å to 3.5 Å (Figure 3). Benefitting from this packing habit, the molecular dipole moments of neighboring molecules are confined in the dimeric pair. This leads to a net dipole moment of zero, giving a reduced bulk dipole for suppressing the formation of deep carrier traps as proposed previously.[39–40]

Theoretical analyses of **CPNT**, **DCPNT**, **CPNBT** and **DCPNBT** were conducted with density functional theory (DFT)[41–42] and time-depend density functional theory (TD-DFT)[43], which were

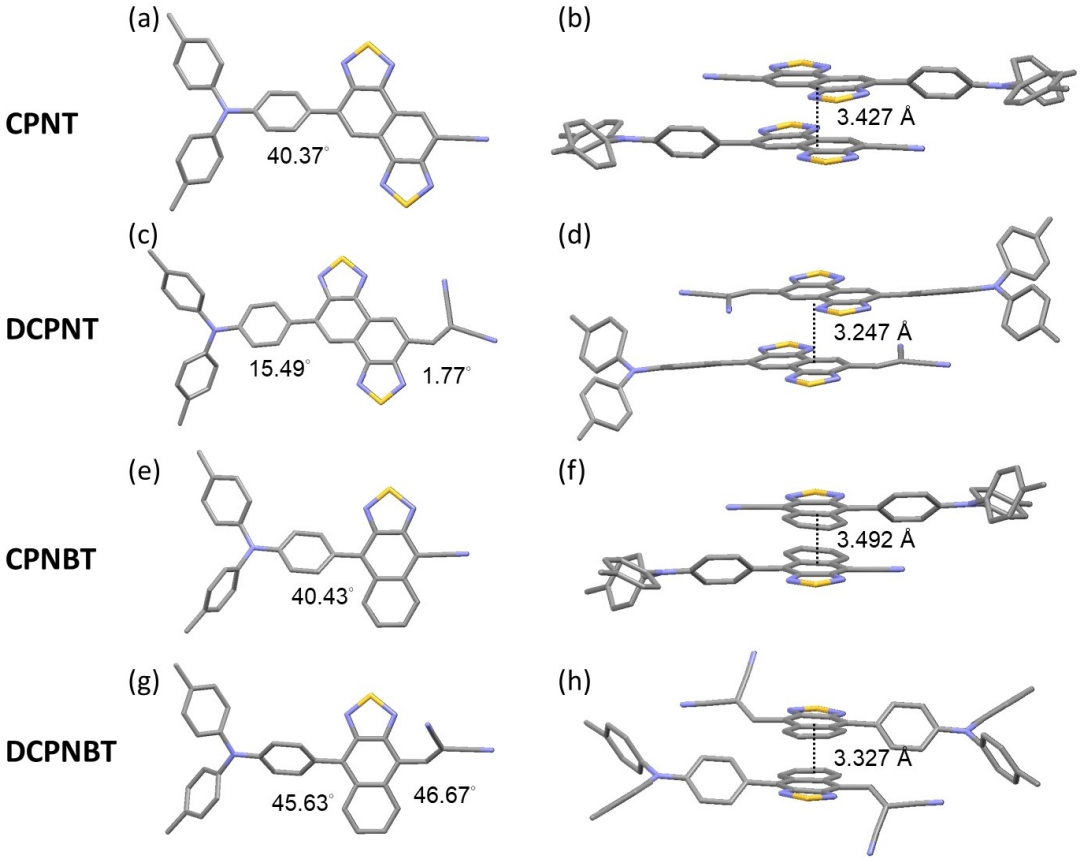

Figure 3. The front view (a, c, e, g) and the antiparallel packing (b, d, f, h) of **CPNT**, **DCPNT**, **CPNBT**, **DCPNBT** crystal structures.

carried out at the long-range corrected ω-B97XD/6-31G(d,p) level[44] in the gaseous state with Gaussian 09 program suite[45]. The coordinates for the calculations were extracted from the respective single crystal structure. The population of HOMO-1, HOMO and LUMO of **CPNT**, **DCPNT**, **CPNBT** and **DCPNBT** are depicted in Figure 4 and the TD-DFT results are summarized in Table 2. As depicted in Figure 4, the HOMOs are mainly distributed on the electron-donating moieties for **CPNT** and **DCPNT**. However, the HOMOs are partially extended to the electron-withdrawing core of **CPNBT** and **DCPNBT**. On the other hand, the LUMOs are mainly distributed on the electron-withdrawing cores NT and NBT coupling to the terminal CN and dicyanovinylene groups for **CPNT**, **DCPNT**, **CPNBT** and **DCPNBT**.

The TD-DFT calculations were conducted to understand the electronic transition of the D-A-A′-configured molecules, with results summarized in Table 2. The $S_1 \leftarrow S_0$ transition is mainly dominated by the HOMO to LUMO transition, with partial contribution coming from the HOMO-1 to LUMO transition. The natural transition orbitals (NTOs) were calculated to analyze the nature of $S_1 \leftarrow S_0$ for **CPNT**, **DCPNT**, **CPNBT** and **DCPNBT**. The hole NTOs and particle NTOs are depicted in Figure 5. The complementary contribution of the triarylamine donor in the hole NTOs relative to the dicyanovinylene/cyano group in the particle NTOs of **CPNT**, **DCPNT**, **CPNBT** and **DCPNBT** indicate the intramolecular charge-transfer nature of the S_0 to S_1 transitions. Moreover, the improved overlap of the hole NTO

Table 2. The electronic transition character of **CPNT**, **DCPNT**, **CPNBT** and **DCPNBT** calculated by TD-DFT.

Molecule	Electronic transition	E [eV, nm])	Composition	Oscillator strength
CPNT	$S_1 \leftarrow S_0$	2.91, 425.4	LUMO←HOMO (70.8%) LUMO←HOMO-1 (21.7%) LUMO + 1←HOMO (2.4%)	0.6739
DCPNT	$S_1 \leftarrow S_0$	2.53, 490.6	LUMO←HOMO (71.0%) LUMO←HOMO-1 (22.5%)	1.1788
CPNBT	$S_1 \leftarrow S_0$	2.55, 485.7	LUMO←HOMO (77.4%) LUMO←HOMO-1 (20.7%)	0.4387
DCPNBT	$S_1 \leftarrow S_0$	2.48, 499.8	LUMO←HOMO (74.8%) LUMO←HOMO-1 (22.7%)	0.5843

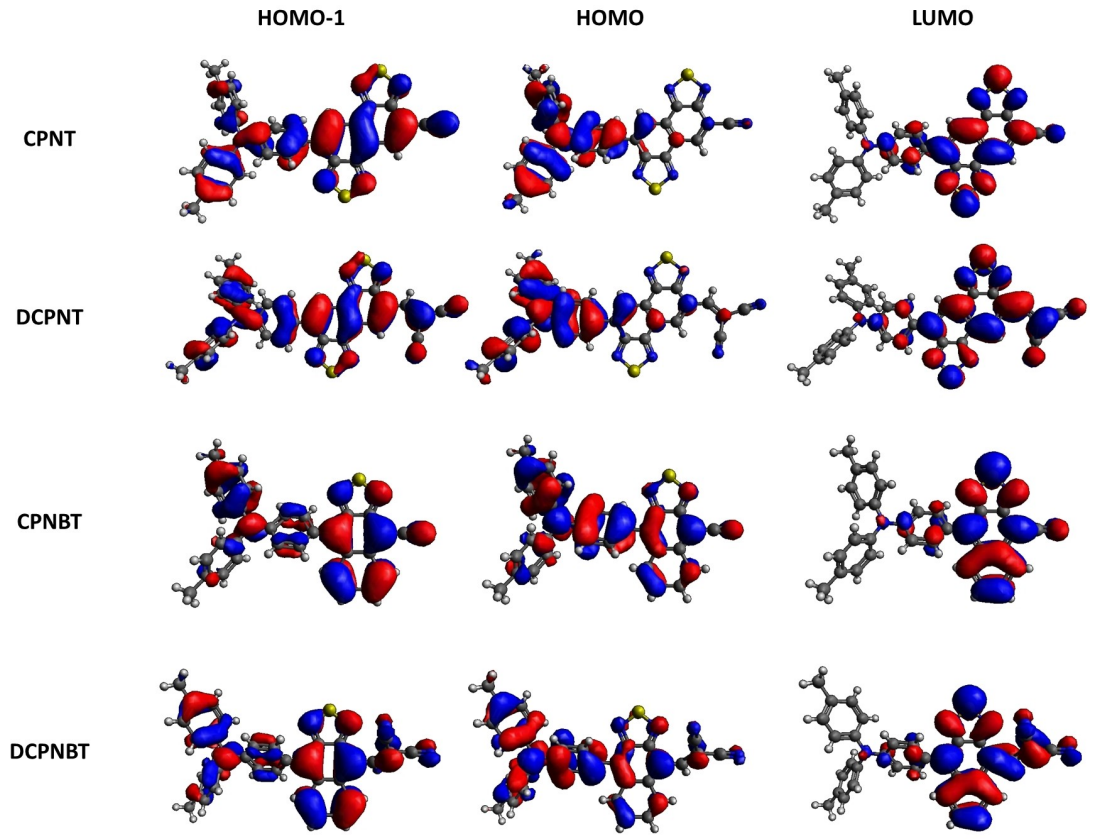

Figure 4. The HOMO-1, HOMO and LUMO distribution of **CPNT**, **DCPNT**, **CPNBT** and **DCPNBT**.

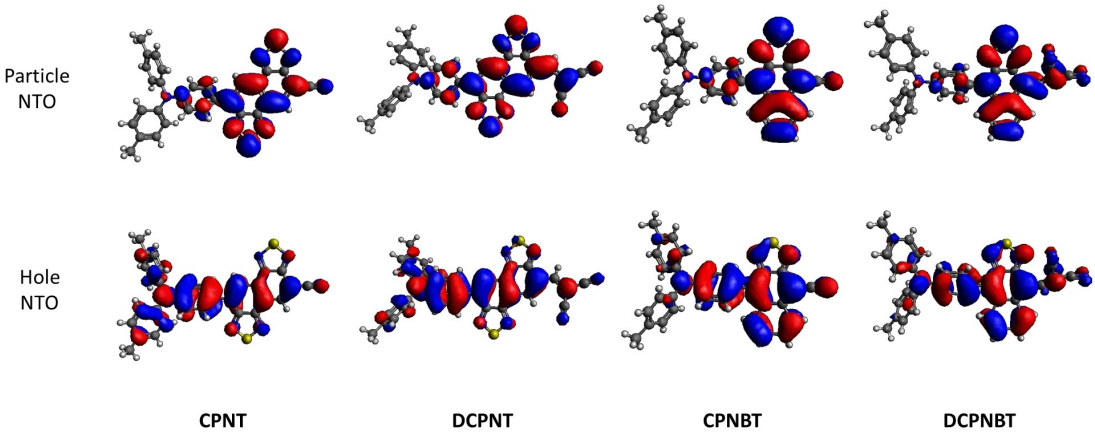

Figure 5. The hole NTOs and particle NTOs of S_0 to S_1 transition of **CPNT**, **DCPNT**, **CPNBT** and **DCPNBT**.

and the particle NTO ensures a larger transition oscillator strength. The replacement of NT with NBT yields twisted structures that interrupt the overlap of the frontier molecular orbitals and, therefore, result in the electronic transition with the smaller oscillator strengths for the NBT-based cases. As a result, NBT-based analogues exhibit lower extinction coefficients of the UV-Vis absorption than their NT-based analogues **CPNT** and **DCPNT**. Nevertheless, **CPNBT** and **DCPNBT** exhibit longer absorption wavelengths owing to better conjugating of the NBT core than their NT-based counterparts. Apparently, the ICT character with a larger oscillator strength is anticipated when the electron deficiency of the terminal electron acceptor is enhanced, namely, changing the cyano group to dicyanovinylene group, leading to the red-shifted absorption with a larger extinction coefficient.

The photovoltaic characteristics of vacuum-deposited OPVs with the active layers comprising D-A-A′ donors and fullerene C_{70} acceptor were explored. Devices were fabricated with the structure configured as indium tin oxide (ITO)/molybdenum (VI) oxide (MoO_3) (15 nm)/donor:C_{70}/bathocuproine (BCP) (6 nm)/Ag

(120 nm). The *J-V* characteristics of optimized devices are shown in Figure 6a, and the corresponding data are summarized in Table 3 with the best *PCE*s presented in parentheses. Among these devices, the **DCPNBT**-based device exhibits inferior *PCE* than those of **CPNT**-, **CPNBT**- and **DCPNT**-based devices. Since all donor molecules have similar HOMO energy levels, the low V_{oc} of **DCPNBT**-based device implies the possibility of severe exciton recombination occurred in the **DCPNBT**:C_{70} blend. In addition, the J_{sc} and *FF* of **DCPNBT**-based device are also much lower than those of other devices, which is ascribed to the lower extinction coefficient and weak π-π interaction, respectively, due to the highly twisted conformation (Figure 3g). Figure 6b shows the external quantum efficiency (*EQE*) spectra of all devices. The device based on **DCPNT** exhibited the highest J_{sc} as compared to those of the devices based on **CPNT**, **CPNBT** and **DCPNBT**. The high extinction coefficient together with close molecular packing of **DCPNT** is plausibly responsible to the higher photocurrents in the region of 650–800 nm. As a result, **DCPNT**-based device displays the highest *PCE* = 6.9%, J_{sc} = 12.59 mA cm^{-2}, V_{oc} = 0.92 V, and *FF* = 0.60. Further optimization of **DCPNT**-based device with the structure configured as ITO/MoO_3 (10 nm)/**DCPNT**:C_{70} (1:3, w/w, 60 nm)/bathophenathroline (BPhen) (5 nm)/Ag (100 nm) led to *PCE* = 8.3%, along with a J_{sc} = 14.5 mA cm^{-2}, V_{oc} = 0.92 V, and *FF* = 0.62.

Hence, the stability of device based on **CPNT**, **CPNBT**- and **DCPNT** as donor and C_{70} as acceptor was examined under continuous light soaking with simulated AM 1.5 G illumination (100 mW cm^2). Figure 7a depicts the real time tracking data of *PCE*, J_{sc}, V_{oc}, and *FF* of these OPVs. As indicated, the *PCE* of **CPNT** and **DCPNT**-based OPVs is found to retain 97% and 91% of the initial value after 150 h, respectively. However, the **CPNBT**-based device only exhibited moderate stability, with 78% remaining relative to its initial *PCE* owing to the drop of V_{oc} during burn-in.[46]

Recently, an OPV has been reported to achieve the best *PCE* up to 28.1% under indoor lighting[47], implying OPV for indoor photovoltaic[48] is an attractive application. The indoor performance of the **CPNT**-, **CPNBT**- and **DCPNT**-based devices were examined under the 500 and 1000 lux illumination of a TLD-840 fluorescent lamp. The *J-V* characteristics of optimized devices are shown in Figure 7b, and the corresponding data are summarized in Table 4. The **CPNT**- and **DCPNT**-based devices exhibit the maximum *PCE* = 12.8% and 12.6% under a 500 lux (145.05 μW cm^{-2}) illumination. However, a moderate *PCE* = 8.4% was achieved for the **CPNBT**-based device, which was marginally increased to 9.0% as the illumination power was 290.12 μW cm^{-2}. The higher PCE of the OPV device under indoor lighting conditions can be attributed to the emission spectrum difference between 1 sun AM 1.5G solar simulator and fluorescent lamp (see Figure S2 in SI for experimental details). The fluorescent lamp shows several emission peaks in the visible region spanning from 400 nm to 750 nm without ultraviolet or near-infrared emission. Thus, a lower radiation energy is obtained using a fluorescent lamp as compared to that employing with the solar simulator. The low V_{oc} of **CPNBT**-based device as compared to those of **CPNT**- and **DCPNT**-based devices indicates the possibility of trap-assisted recombination in **CPNBT**:C_{70} blend under the illumination of an indoor light.

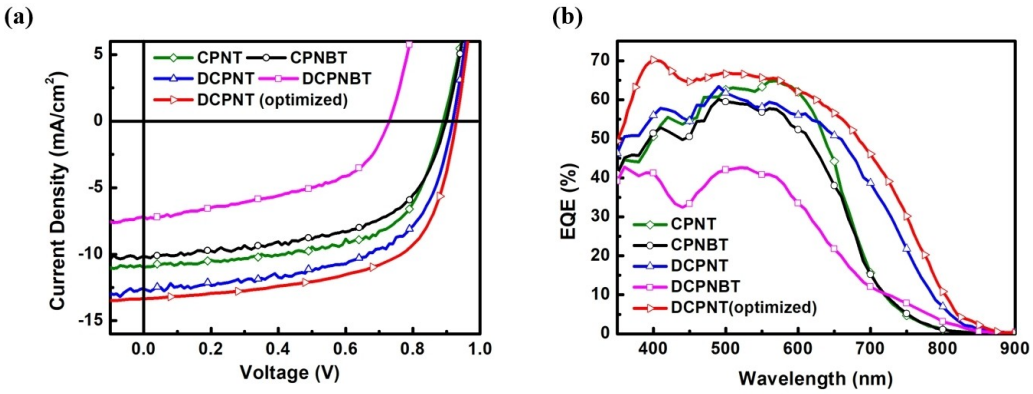

Figure 6. (a) *J-V* characteristics and (b) *EQE* spectra of **CPNT**-, **CPNBT**-, **DCPNT**- and **DCPNBT**-based devices.

Table 3. Device parameters of **CPNT**-, **CPNBT**-, **DCPNT**- and **DCPNBT**-based devices under 1 sun illumination.

Device[a] (donor:C_{70})	J_{sc} [mA cm^{-2}]	V_{oc} [V]	FF	*PCE*[c] [%]	R_{sh} [kΩ cm^2]	R_s [Ω cm^2]
CPNT (1:1, 70 nm)	10.54 ± 0.45	0.89 ± 0.01	0.58 ± 0.02	5.4 ± 0.5 (5.9)	0.33 ± 0.02	3.14 ± 0.02
CPNBT (1:3, 60 nm)	9.76 ± 0.37	0.89 ± 0.01	0.56 ± 0.02	4.8 ± 0.4 (5.2)	0.34 ± 0.02	3.82 ± 0.02
DCPNT (1:2, 60 nm)	12.59 ± 0.31	0.91 ± 0.01	0.58 ± 0.02	6.7 ± 0.3 (6.9)	0.33 ± 0.02	3.14 ± 0.02
DCPNT[b] (1:3, 60 nm)	14.26 ± 0.24	0.91 ± 0.01	0.60 ± 0.02	7.8 ± 0.5 (8.3)	-	-
DCPNBT(1:3, 40 nm)	6.14 ± 1.53	0.70 ± 0.03	0.46 ± 0.03	2.0 ± 0.6 (2.6)	0.35 ± 0.12	4.45 ± 1.40

[a] Optimized with device structure configured as ITO/MoO_3 (15 nm)/**donor**:C_{70} (mixing ratio w/w, thickness)/BCP (6 nm)/Ag (120 nm). [b] The device structure configured as ITO/MoO_3 (10 nm)/**DCPNT**:C_{70} (mixing ratio w/w, thickness)/BPhen (5 nm)/Ag (100 nm) for further optimization. [c] The values in the parenthesis are the highest *PCE*.

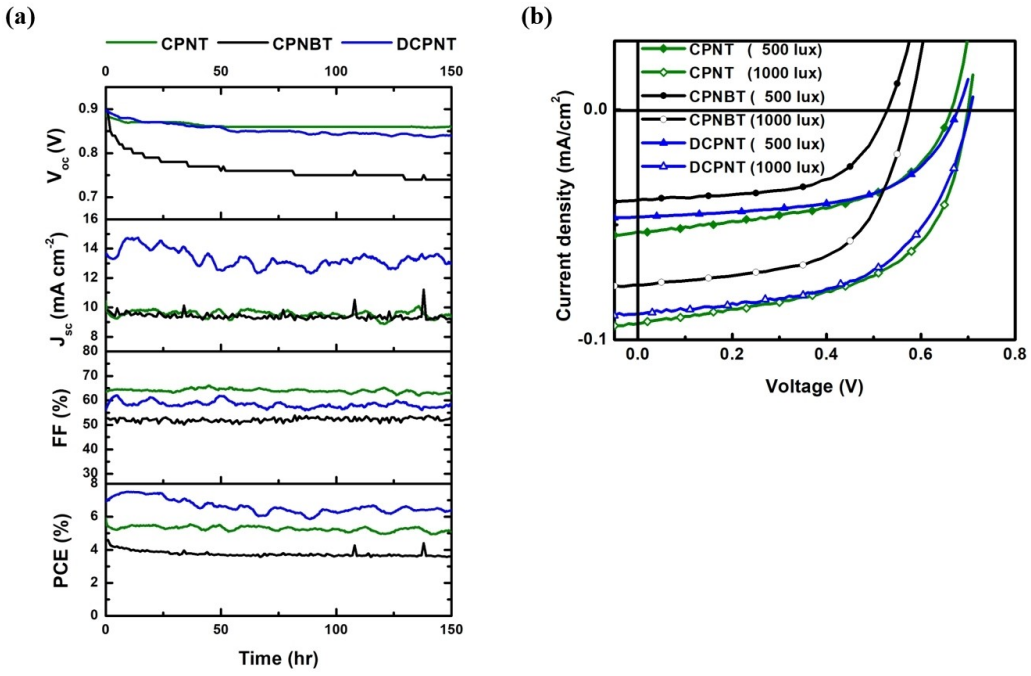

Figure 7. (a) Characteristics of **CPNT**-, **CPNBT**- and **DCPNT**-based devices under continuous AM 1.5G illumination in ambient room. (b) *J-V* characteristics of **CPNT**-, **CPNBT**- and **DCPNT**-based devices under illumination of TLD-840 fluorescent lamp with 500 and 1000 lux.

Table 4. Device parameters of **CPNT**-, **CPNBT**-, **DCPNT**- and **DCPNBT**-based devices under illumination of TLD-840 fluorescent lamp with 500 and 1000 lux.

Device (irradiation intensity)	J_{sc} [μA cm^{-2}]	V_{oc} [V]	FF	*PCE* [%]	P_{in} [μW cm^{-2}]
CPNT (500 lux)	53.4 ± 0.1	0.666 ± 0.001	0.516 ± 0.003	12.7 ± 0.1 (12.8)	145.05
CPNT (1000 lux)	92.9 ± 0.2	0.701 ± 0.001	0.556 ± 0.002	12.5 ± 0.1 (12.6)	290.12
CPNBT (500 lux)	39.2 ± 0.3	0.532 ± 0.001	0.577 ± 0.004	8.3 ± 0.1 (8.4)	145.05
CPNBT (1000 lux)	76.1 ± 0.1	0.574 ± 0.001	0.591 ± 0.002	8.9 ± 0.1 (9.0)	290.12
DCPNT(500 lux)	46.6 ± 0.0	0.679 ± 0.001	0.573 ± 0.001	12.5 ± 0.0 (12.5)	145.05
DCPNT(1000 lux)	88.8 ± 0.2	0.708 ± 0.001	0.564 ± 0.004	12.2 ± 0.1 (12.3)	290.12

These results imply that the introduction of NBT as the central A component of the D-A-A′-configured molecule leads to highly twisted molecular structure that reduces the oscillator strength of ICT absorption as well as intermolecular coupling. As a result, lower *PCE* as well as reduced lifetime of the OPV device based on the NBT derivatives is found, compared to donors incorporating NT derivatives. Encouragingly, the **CPNT**- and **DCPNT**-based vacuum-processed OPVs exhibit high indoor *PCE*s with good device lifetime may show the potential to meet the requirement of long-term indoor application.

Conclusion

In summary, two electron-deficient building blocks NT and NBT, exhibit strong electron-deficiency together with the extended conjugation, have been introduced as the central A moiety of D-A-A′-configured molecular skeletons for modulating the physical properties of the resulting D-A-A′-type molecules as compared to those of BT-based parent molecules. A new synthetic pathway combining Suzuki cross-coupling and ozonolysis afforded the crucial bromo carboxaldehyde derivatives of NT and NBT building blocks, paving a way for synthesizing asymmetric D-A-A′-type molecules. Triarylamino group was adopted as the D group of four D-A-A′-type molecules, in which **CPNT** and **CPNBT** with cyano as the terminal A group, **DCPNT** and **DCPNBT** with dicyanovinylene as the end-capped A group, were synthesized and characterized. The substitution of BT moiety with NT and NBT moieties having better quinoidal and electron-deficient characters results in red-shifted absorptions due to the lower LUMO energy levels and thus the stronger molecular ICT character. Among these molecules, **DCPNBT** exhibits the most red-shifted ICT absorption (λ_{onset} = 722 nm), indicating that the introduction of NBT moiety is more effective for D-A-A′ molecule reaching to NIR absorption than BT and NT. However, the lower extinction coefficient, inferior thermal stability and weak π-π interactions of **DCPNBT** ascribed to the twisted conformation observed both in theoretical calculations and in X-ray structure analysis impedes its application as donor for vacuum-deposited OPV. The blends comprising the D-A-A′ molecules **CPNT**, **CPNBT**, and **DCPNT** as donors and C_{70} as acceptor were examined as the active layers of vacuum-

deposited OPV devices. After optimization, the device employed **DCPNBT**:C_{70} as the active layer showed *PCE* = 2.6%, while the device employed **DCPNT**:C_{70} blend displayed the best *PCE* = 8.3%, along with V_{oc} = 0.92 V, J_{sc} = 14.5 mA cm^{-2} and *FF* = 62%. Furthermore, the devices based on **CPNT** and **DCPNT** displayed high stability upon the continuous AM 1.5G illumination as compared to that of the **CPNBT**-based device. The further application of the vacuum-processed OPVs for indoor light harvesting was explored. In this regard, the **CPNT**- and **DCPNT**-based devices exhibited *PCE* = 12.8% and 12.6%, respectively, under 500 lux illumination of a TLD-840 fluorescent lamp, while the **CPNBT**-based device only displayed maximum *PCE* = 9.0%. These results indicate that **CPNT** and **DCPNT** are promising candidates for giving the vacuum-deposited OPVs with high-stability and potential application for indoor-light harvesting.

ACKNOWLEDGMENT

We thank the Ministry of Science and Technology of Taiwan (MOST 106-2628-E-131-001-MY2; MOST 107-2113-M-002-019-MY3), Academia Sinica (AS-SS-106-02, AS-SS-106-02), and Featured Area Research Center Program within the framework of the Higher Education Sprout Project by the Ministry of Education (107 L9006) for financial support. The support from the National Science Foundation Award No. 1905401 (X.C., experiment, analysis; S.R.F., analysis), the Department of the Navy, Office of Naval Research under award no. N00014-17-1-2211 (K.D., X.L., experiment, analysis) and Universal Display Corp. is also acknowledged. We thank the Instrumentation Center of National Taiwan University for the thermogravimetric analysis (TGA), differential scanning calorimetry (DSC) analysis and the single crystal structure determinations. We are grateful to the National Center for High-performance Computing for computer time and facilities and Mass Spectrometry-based Proteomics Core Facility of Department of Chemistry in National Taiwan University.

Conflict of Interest

The authors declare no conflict of interest.

Keywords: organic photovoltaic · vacuum process · small molecule donor · indoor photovoltaic

[1] S. B. Darling, F. You, *RSC Adv.* **2013**, *3*, 17633–17648.
[2] L. Lu, T. Zheng, Q. Wu, A. M. Schneider, D. Zhao, L. Yu, *Chem. Rev.* **2015**, *115*, 12666–12731.
[3] Y. J. Cheng, S. H. Yang, C. S. Hsu, *Chem. Rev.* **2009**, *109*, 5868–5923.
[4] H. Kang, G. Kim, J. Kim, S. Kwon, H. Kim, K. Lee, *Adv. Mater.* **2016**, *28*, 7821–7861.
[5] G. Li, R. Zhu, Y. Yang, *Nat. Photonics* **2012**, *6*, 153–161.
[6] B. Kan, M. Li, Q. Zhang, F. Liu, X. Wan, Y. Wang, W. Ni, G. Long, X. Yang, H. Feng, Y. Zuo, M. Zhang, F. Huang, Y. Cao, T. P. Russell, Y. Chen, *J. Am. Chem. Soc.* **2015**, *137*, 3886–3893.
[7] D. Deng, Y. Zhang, J. Zhang, Z. Wang, L. Zhu, J. Fang, B. Xia, Z. Wang, K. Lu, W. Ma, Z. Wei, *Nat. Commun.* **2016**, *7*, 13740.
[8] Y. Liu, J. Zhao, Z. Li, C. Mu, W. Ma, H. Hu, K. Jiang, H. Lin, H. Ade, H. Yan, *Nat. Commun.* **2014**, *5*, 5293.
[9] J. Zhao, Y. Li, G. Yang, K. Jiang, H. Lin, H. Ade, W. Ma, H. Yan, *Nat. Energy* **2016**, *1*, 15027.
[10] A. Venkateswararao, S.-W. Liu, K.-T. Wong, *Mater. Sci. Eng. R Rep.* **2018**, *124*, 1–57.
[11] S. Li, W. Liu, C. Z. Li, M. Shi, H. Chen, *Small* **2017**, *13*, 1701120.
[12] H. Sun, F. Chen, Z.-K. Chen, *Mater. Today* **2019**, *24*, 94–118.
[13] C. Yan, S. Barlow, Z. Wang, H. Yan, A. K. Y. Jen, S. R. Marder, X. Zhan, *Nat. Rev. Mater.* **2018**, *3*, 18003.
[14] G. Zhang, J. Zhao, P. C. Y. Chow, K. Jiang, J. Zhang, Z. Zhu, J. Zhang, F. Huang, H. Yan, *Chem. Rev.* **2018**, *118*, 3447–3507.
[15] Y. Lin, Z.-G. Zhang, H. Bai, J. Wang, Y. Yao, Y. Li, D. Zhu, X. Zhan, *Energy Environ. Sci.* **2015**, *8*, 610–616.
[16] Y. Wu, Y. Zheng, H. Yang, C. Sun, Y. Dong, C. Cui, H. Yan, Y. Li, *Sci. China Chem.* **2020**, *63*, 265–271.
[17] L. Liu, Y. Kan, K. Gao, J. Wang, M. Zhao, H. Chen, C. Zhao, T. Jiu, A. K. Jen, Y. Li, *Adv. Mater.* **2020**, *32*, 1907604.
[18] R. Ma, T. Liu, Z. Luo, Q. Guo, Y. Xiao, Y. Chen, X. Li, S. Luo, X. Lu, M. Zhang, Y. Li, H. Yan, *Sci. China Chem.* **2020**, *63*, 325–330.
[19] Z. Zhou, W. Liu, G. Zhou, M. Zhang, D. Qian, J. Zhang, S. Chen, S. Xu, C. Yang, F. Gao, H. Zhu, F. Liu, X. Zhu, *Adv. Mater.* **2019**, 1906324.
[20] B. Fan, D. Zhang, M. Li, W. Zhong, Z. Zeng, L. Ying, F. Huang, Y. Cao, *Sci. China Chem.* **2019**, *62*, 746–752.
[21] Y. Cui, H. Yao, J. Zhang, T. Zhang, Y. Wang, L. Hong, K. Xian, B. Xu, S. Zhang, J. Peng, *Nat. Commun.* **2019**, *10*, 2515.
[22] Q. Liu, Y. Jiang, K. Jin, J. Qin, J. Xu, W. Li, J. Xiong, J. Liu, Z. Xiao, K. Sun, S. Yang, X. Zhang, L. Ding, *Sci. Bull.* **2020**, *65*, 272–275.
[23] P. Cheng, X. Zhan, *Chem. Soc. Rev.* **2016**, *45*, 2544–2582.
[24] C. I. Park, M. Seong, M. A. Kim, D. Kim, H. Jung, M. Cho, S. H. Lee, H. Lee, S. Min, J. Kim, M. Kim, J.-H. Park, S. Kwon, B. Kim, S. J. Kim, W. Park, J.-Y. Yang, S. Yoon, I. Kang, *J. Soc. Inf. Disp.* **2018**, *26*, 287–295.
[25] Q. Burlingame, X. Huang, X. Liu, C. Jeong, C. Coburn, S. R. Forrest, *Nature* **2019**, *573*, 394–397.
[26] C. H. Chen, H. C. Ting, Y. Z. Li, Y. C. Lo, P. H. Sher, J. K. Wang, T. L. Chiu, C. F. Lin, I. S. Hsu, J. H. Lee, S. W. Liu, K. T. Wong, *ACS Appl. Mater. Interfaces* **2019**, *11*, 8337–8349.
[27] Y. H. Chen, L. Y. Lin, C. W. Lu, F. Lin, Z. Y. Huang, H. W. Lin, P. H. Wang, Y. H. Liu, K. T. Wong, J. Wen, D. J. Miller, S. B. Darling, *J. Am. Chem. Soc.* **2012**, *134*, 13616–13623.
[28] X. Che, Y. Li, Y. Qu, S. R. Forrest, *Nat. Energy* **2018**, *3*, 422–427.
[29] I. Osaka, M. Shimawaki, H. Mori, I. Doi, E. Miyazaki, T. Koganezawa, K. Takimiya, *J. Am. Chem. Soc.* **2012**, *134*, 3498–3507.
[30] I. Osaka, T. Kakara, N. Takemura, T. Koganezawa, K. Takimiya, *J. Am. Chem. Soc.* **2013**, *135*, 8834–8837.
[31] M. Saito, I. Osaka, Y. Suzuki, K. Takimiya, T. Okabe, S. Ikeda, T. Asano, *Sci. Rep.* **2015**, *5*, 14202.
[32] F.-Y. Cao, C.-C. Tseng, F.-Y. Lin, Y. Chen, H. Yan, Y.-J. Cheng, *Chem. Mater.* **2017**, *29*, 10045–10052.
[33] X. Tang, X.-L. Li, H. Liu, Y. Gao, Y. Shen, S. Zhang, P. Lu, B. Yang, S.-J. Su, Y. Ma, *Dyes Pigm.* **2018**, *149*, 430–436.
[34] Y. C. Lo, T. H. Yeh, C. K. Wang, B. J. Peng, J. L. Hsieh, C. C. Lee, S. W. Liu, K. T. Wong, *ACS Appl. Mater. Interfaces* **2019**, *11*, 23417–23427.
[35] J. Kim, M. H. Yun, G.-H. Kim, J. Y. Kim, C. Yang, *Polym. Chem.* **2012**, *3*, 3276–3281.
[36] P. Shen, H. Bin, L. Chen, Z.-G. Zhang, Y. Li, *Polymer* **2015**, *79*, 119–127.
[37] K. Kawashima, I. Osaka, K. Takimiya, *Chem. Mater.* **2015**, *27*, 6558–6570.
[38] P. M. Burrezo, J. L. Zafra, J. T. Lopez Navarrete, J. Casado, *Angew. Chem. Int. Ed.* **2017**, *56*, 2250–2259; *Angew. Chem.* **2017**, *129*, 2286–2296.
[39] V. Steinmann, N. M. Kronenberg, M. R. Lenze, S. M. Graf, D. Hertel, K. Meerholz, H. Bürckstümmer, E. V. Tulyakova, F. Würthner, *Adv. Energy Mater.* **2011**, *1*, 888–893.
[40] A. Arjona-Esteban, J. Krumrain, A. Liess, M. Stolte, L. Huang, D. Schmidt, V. Stepanenko, M. Gsanger, D. Hertel, K. Meerholz, F. Wurthner, *J. Am. Chem. Soc.* **2015**, *137*, 13524–13534.
[41] P. Hohenberg, W. Kohn, *Phys. Rev.* **1964**, *136*, B864-B871.
[42] W. Kohn, L. J. Sham, *Phys. Rev.* **1965**, *140*, A1133-A1138.
[43] E. Runge, E. K. U. Gross, *Phys. Rev. Lett.* **1984**, *52*, 997–1000.
[44] J. D. Chai, M. Head-Gordon, *Phys. Chem. Chem. Phys.* **2008**, *10*, 6615–6620.
[45] M. J. Frisch, G. W. Trucks, H. B. Schlegel, G. E. Scuseria, M. A. Robb, J. R. Cheeseman, G. Scalmani, V. Barone, B. Mennucci, G. A. Petersson, H. Nakatsuji, M. Caricato, X. Li, H. P. Hratchian, A. F. Izmaylov, J. Bloino, G. Zheng, J. L. Sonnenberg, M. Hada, M. Ehara, K. Toyota, R. Fukuda, J. Hasegawa, M. Ishida, T. Nakajima, Y. Honda, O. Kitao, H. Nakai, T. Vreven, J. J. A. Montgomery, F. O. J. E. Peralta, M. Bearpark, E. B. J. J. Heyd, K. N. Kudin, V. N. Staroverov, R. Kobayashi, J. Normand, K. Raghavachari, A.

Rendell, J. C. Burant, S. S. Iyengar, J. T. M. Cossi, N. Rega, J. M. Millam, M. Klene, J. E. Knox, J. B. Cross, V. Bakken, C. Adamo, J. Jaramillo, R. Gomperts, R. E. Stratmann, O. Yazyev, A. J. Austin, R. Cammi, C. Pomelli, J. W. Ochterski, R. L. Martin, K. Morokuma, V. G. Zakrzewski, G. A. Voth, P. Salvador, J. J. Dannenberg, S. Dapprich, A. D. Daniels, Ö. Farkas, J. B. Foresman, J. V. Ortiz, J. Cioslowski, D. J. Fox, *Gaussian 09*, Gaussian, Inc., Wallingford CT, 2009.

[46] C. H. Peters, I. T. Sachs-Quintana, J. P. Kastrop, S. Beaupré, M. Leclerc, M. D. McGehee, *Adv. Energy Mater.* **2011**, *1*, 491–494.

[47] H. K. H. Lee, J. Wu, J. Barbé, S. M. Jain, S. Wood, E. M. Speller, Z. Li, F. A. Castro, J. R. Durrant, W. C. Tsoi, *J. Mater. Chem. A* **2018**, *6*, 5618–5626.

[48] A. Venkateswararao, J. K. W. Ho, S. K. So, S.-W. Liu, K.-T. Wong, *Mater. Sci. Eng. R* **2020**, *139*, 100517.

Manuscript received: May 26, 2020
Revised manuscript received: June 18, 2020
Accepted manuscript online: June 22, 2020
Version of record online: July 6, 2020